Secondary Kinetic Isotope Effect in Nucleophilic Substitution: A Quantum-Mechanical Approach†

Carsten Hennig, Rainer B. Oswald, and Stefan Schmatz*

Institut für Physikalische Chemie, Universität Göttingen, Tammannstrasse 6, D-37077 Göttingen, Germany

Received: July 20, 2005; In Final Form: September 14, 2005

Four-dimensional time-independent quantum scattering calculations have been carried out on the perdeuterated exothermic and complex-forming gas-phase S_N2 reaction $Cl^- + CD_3Br \rightarrow ClCD_3 + Br^-$ and the reverse process $Br^- + CD_3Cl \rightarrow BrCD_3 + Cl^-$, employing a fine energetic resolution to resolve all scattering resonances. The two totally symmetric modes of the methyl group, C−D symmetric stretch and umbrella bend, are explicitly taken into account. Converged state-selected reaction probabilities and product distributions have been calculated up to 2960 cm^{-1} above the vibrational ground state of CD_3Br, i.e., up to initial vibrational excitation of the second overtone of the umbrella bending vibration. The inverse secondary kinetic isotope effect found experimentally is nicely confirmed by the calculated state-selected reaction probabilities. One contribution to this originates from excitation of the high-frequency symmetric C−D stretching vibration, which increases the reaction probability as a function of translational energy more than the corresponding vibration in the undeuterated system. Although transition state theory (TST) suffices to explain this effect qualitatively, the dynamics of S_N2 reactions is well-known to show strong nonstatistical features. A striking example is given by the umbrella mode: Contrary to estimates obtained from TST, we find a significant enhancement of the reactivity in the perdeuterated system that is attributed to the increased density of states and the higher number of avoided crossings of the hyperspherical adiabats compared to the undeuterated system. Furthermore, compared to the system $Cl^- + CH_3Cl'/CD_3Cl'$, the influence of tunneling is negligible in this net-barrierless reaction. In the reverse endothermic reaction, the kinetic isotope effect of the umbrella mode is normal.

I. Introduction

Kinetic isotope effects (KIEs) are among the most sensitive experimental probes of transition state structures. Secondary KIEs are observed when the isotopically substituted atom is not directly involved in a chemical process, i.e., does not actively take part in bond breaking or bond formation. Rather, the isotopic substitution influences the internal vibrations of the system which in turn can, e.g., via the zero-point energy, change the energetics, in particular the heights of reaction barriers and thus the rates of chemical reactions. Secondary kinetic isotope effects arising from H/D exchange in α-position have been studied for gas-phase S_N2 bimolecular substitutions reactions by experiment[1−6] and theoretically,[2,6−11] employing variational transition state theory (VTST)/canonical variational theory (CVT) and trajectory calculations. Measurements of thermal rate constants[1−5] revealed that an inverse KIE ($k_H/k_D < 1$, where k denotes the rate constant) is characteristic for thermal S_N2 reactions. Theoretically, employing variational transition state calculations including semiempirical transmission coefficients, Zhao, Tucker, and Truhlar[9] could qualitatively explain the observed inverse KIE for the symmetric chlorine exchange reaction. Wang and Hase[7] performed extensive TST calculations on the $Cl^- + CH_3Br$ system, which resulted in a qualitative explanation of the inverse KIE and strong hints for nonstatistical behavior.

As is well-known, inverse KIEs result from isotopically sensitive vibrational modes with frequencies which become higher when proceeding from reactants to the transition state. This is the case for the C−H stretches the frequencies of which increase due to the change of hybridization (from sp^3 to sp^2) and the correspondingly stronger bonding when going from reactants to the transition state. By analyzing the contributions from each vibrational mode, Hu and Truhlar[8] showed that in particular the high-frequency stretching vibrations are the dominant contributors for the inverse effect. This was quite surprising because the common belief was that the bending and particularly the CH_3 deformation vibrations contributed most to the KIE.[12−20] Although conventional TST does not suffice to obtain quantitatively correct rate constants,[7] Hu and Truhlar could also show that the variational effects are negligible in studying the α-deutero secondary KIE in halogen-exchange S_N2 reactions so that among the various transition state theories conventional TST is sufficient.[8] Also, tunneling corrections appear to play only a very minor role.[9]

Although a TST calculation, which is mainly based on the analysis of harmonic vibrational frequencies in reactants and at the transition state, can qualitatively explain the observed inverse KIE, a quantitative agreement is not feasible due to strong nonstatistical effects. Thus, a detailed state-specific quantum-mechanical investigation is highly desirable to understand in depth the underlying dynamic processes.

Gas-phase S_N2 reactions have been studied in detail both experimentally[21−33] and theoretically.[34−66] Due to the ion−dipole attraction between nucleophile and substrate, relatively strongly bound intermediate complexes in the entrance and exit channels are formed. These aggregates are associated with the existence of considerably long-lived Feshbach (and in exothermic systems

† Part of the special issue "Jürgen Troe Festschrift".

* Corresponding author. E-mail: sschmat@gwdg.de.

10.1021/jp0540151 CCC: $33.50
Published on Web 11/08/2005

also shape) resonance states, which continue the bound state spectra of the complexes into the energetic continuum. These resonances dominate the reaction probability.

Recently, the state-selected quantum dynamics of the exothermic gas-phase S_N2 reaction

$$Cl^- + CH_3Br \rightarrow ClCH_3 + Br^- \quad (1)$$

has been investigated in detail within a four-dimensional (4D) model,[56,59,63−65] which includes the two totally symmetric internal vibrations of the methyl group, C−H stretch (ν_1), and umbrella bend (ν_2). The study revealed several unexpected features, among these the importance of the high-frequency C−H stretching mode at low translational energies. Though such modes are usually considered as spectators and thus a priori excluded from the dynamics, calculated product distributions reveal a nonadiabatic behavior of the ν_1 mode. These product distributions also show that those product states are preferred that are energetically close to the internal energies of the reactants.

For reaction 1, employing the flowing afterglow-selected ion flow tube (FA-SIFT) method, the α-deutero KIE was determined by Bierbaum and co-workers[1] to be $k_H/k_D(300\ K) = 0.80 \pm 0.06$. Shortly after its first publication, this value was confirmed by Viggiano et al.,[2] who performed measurement over a larger temperature interval ($207\ K < T < 564\ K$) in a variable-temperature selected ion flow drift tube (VT-SIFDT). For 300 K, the authors obtained $k_H/k_D = 0.81 \pm 0.03$, which is in general agreement with their proposed TST value of 0.93. A more recent measurement by Bierbaum et al.[5] gives an improved and slightly lower value of 0.77 ± 0.03.

These findings stimulate a detailed investigation of the effect of perdeuteration on the $Cl^- + CH_3Br$ reaction. The H/D substitution affects the C−H bending and stretching modes of the methyl group, rendering the corresponding vibrational frequencies considerably smaller.

Our paper is organized as follows: section II briefly summarizes the theoretical and computational foundations from ref 64 and lists the modifications introduced for the perdeuterated reaction, and section III presents the results along with their analysis and discussion. Finally, section IV contains our conclusions. Throughout this work, energies are quoted in wavenumber units.

II. Computational Details

Within the dimensionality-reduced 4D model described in detail in ref 64, we employ a collinear alignment of the three heavy nuclei for the reaction

$$Cl^- + CD_3Br(v_1', v_2', v_3') \rightarrow ClCD_3(v_1, v_2, v_3) + Br^- \quad (2)$$

Here, v_i' and v_i, $i = 1-3$, denote the quantum numbers of the symmetric C−D stretching, the umbrella bending, and the C−Hal stretching vibrational modes in the reactant and product methyl halide molecules, respectively. The 4D CCSD(T) potential energy surface (PES) from ref 63 with classical asymptotic energy set to zero is employed. The scattering problem is formulated in hyperspherical coordinates and solved by first diagonalizing the surface Hamiltonian employing the Lanczos algorithm with partial reorthogonalization[64] and then propagating the one-dimensional translational wave functions (actually the pertinent **R** matrices) along the hyperradius. At asymptotic hyperradii, we apply boundary conditions, extract the **S** matrix, and obtain state-to-state reaction probabilities $P_{i,f}(E)$ as the squared moduli of the corresponding **S** matrix elements, $P_{i,f}(E) = |S_{i,f}(E)|^2$. The **S** matrix contains information about the reactive and nonreactive processes as well as on the reverse reaction. Unless stated otherwise, all energies quoted in this paper are counted from the asymptotic vibrational ground states of either CD_3Br (entrance channel) or CD_3Cl (exit channel).

Several aspects had to be taken into account when the relevant parameters from the nondeuterated reaction (cf. ref 64) were adapted. The higher density of states required the number of computed eigenstates in each sector to be increased to $N_{ch} = 250$; the number of sectors remained unchanged at $N_{sect} = 300$, equally distributed between $\rho_{min} = 8.2\ a_0$ and $\rho_{max} = 34\ a_0$. To obtain convergence of the eigenstates, the DVR basis had to be increased as well: $N_\delta = 1250$ sinc-DVR and $n_\delta = 100$ PO-DVR points, respectively, determine the size of the grid for the hyperangle, where the ratio $N_\delta/n_\delta = 12.5$ was retained. Similarly to the undeuterated system, the two coordinates q und z used to describe the methyl group needed a much smaller ratio between the basic and the optimized grid of only four while the size increased to $N_z = 240$, $n_z = 60$, $N_q = 80$, and $n_q = 20$. The considerably higher grid density in the umbrella mode compared to the carbon−hydrogen stretch is maintained from the undeuterated system as well, reflecting the coupling of the umbrella and the C−Hal stretching modes (note that the energetic spacing of the modes is now approximately 1:1.5:3). As in the investigation of the deuteration in the chlorine−chlorine exchange reaction,[60] the N_q value is larger than that used for the $Cl^- + CH_3Br$ system due to the smaller de Broglie wavelength of the C−D stretching motion. After discarding all points above $V_{cut} = 24200\ cm^{-1}$, the effective size of the resulting 3D Hamiltonian was considerably increased with respect to the undeuterated system, varying between $N^{PO} = 71\,480$ in the minimum of the potential and $N^{PO} = 48\,919$ in the asymptotic region.

In the **R** matrix propagation, in each sector, a local energy-dependent number of channels was used similar to refs 59 and 64. All open channels and 10 additional closed channels were considered. In the potential wells, fewer channels had to be chosen for high energies because the energetically highest computed state in this region lies at ca. 4030 cm^{-1} total energy, i.e., ca. 1400 cm^{-1} above the asymptotic vibrational ground state of CD_3Br. Considering this restriction, all channels below a total energy of 4000 cm^{-1} were additionally included in each sector in computations with an energy below that limit.

Due to the increased density of states, the energy range for which **S** matrices and thus reaction probabilities have been computed was lowered to to 2960 cm^{-1} above the asymptotic vibrational ground state of CD_3Br. This is ca. 75% of the chosen energy range of the nondeuterated reaction while the same number of final asymptotic states (61) was achieved. The energetic resolution was at least 10^{-3} cm^{-1} up to an energy of ca. 2510 cm^{-1}. To resolve the resonances, the algorithm described in ref 59 was employed in this energetic region. Above 2510 cm^{-1}, an equidistant grid of 10^{-2} cm^{-1} was used as no narrow resonances are expected for these energies and the computational effort rises strongly with the increased density of states especially in the potential well.

III. Results and Discussion

A. Exothermic Reaction $Cl^- + CD_3Br$. Harmonic vibrational frequencies for the five stationary points of the reactive system $Cl^- + CD_3Br$ are quoted in Table 1. They were calculated by employing the local potential energy functions that were already used to determine the frequencies of the

TABLE 1: Harmonic Vibrational Frequencies (cm^{-1}) of the System $[ClCD_3Br]^-$ [a]

		$Cl^- + CD_3Br$	$Cl^-\cdots CD_3Br$	$[Cl\cdots CD_3\cdots Br]^-$	$ClCD_3\cdots Br^-$	$ClCD_3 + Br^-$
ω_1 (a_1)	symmetric C−D stretch	2211	2231	2248	2224	2202
ω_2 (a_1)	umbrella bend	1012	949	731	1000	1049
ω_3 (a_1)	intramolecular C−Hal stretch[b]	587	508	186	635	707
ω_4 (a_1)	intermolecular C−Hal stretch[c]		101	450 *i*	82	
ω_5 (e)	antisymmetric C−D stretch	2375	2411	2542	2401	2363
ω_6 (e)	antisymmetric C−D bend	1077	1076	1048	1091	1086
ω_7 (e)	CD_3 rock	731	690	705	750	777
ω_8 (e)	intermolecular C−Hal bend		67	166	67	

[a] CCSD(T) results obtained employing the local potential energy functions from ref 68. [b] Symmetric Cl−C−Br stretch at the transition state. [c] Transitional mode in the transition state.

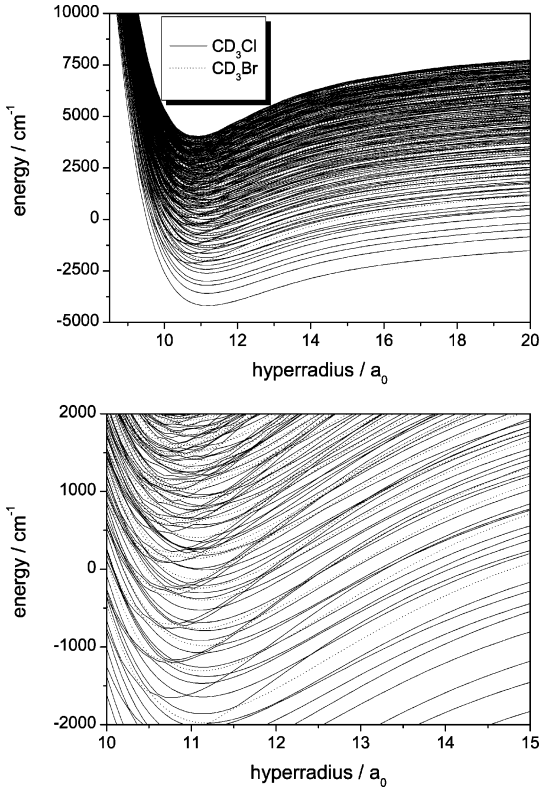

Figure 1. Hyperspherical adiabatic curves for the reactive system $Cl^- + CD_3Br$. Shown are 250 curves of which 162 belong to asymptotic exit channel states and the remaining 88 are associated with entrance channel states. The classical asymptotic limit of the PES is set to zero. The top figure gives an overview, while the bottom figure displays only a small part that includes many avoided crossings between the curves that mediate transitions between the different adiabatic vibrational states. Note that the curves in the top figure are plotted only up to hyperradii of 20 a_0 whereas the actual calculations extend to 34 a_0. The lowest curve approaches the zero point vibrational energy of free CD_3Br for large ρ (cf. Table 2).

$Cl^- + CH_3Br$ system.[68] The values ω_1 and ω_2 are considerably lower than those in the undeuterated system, and the correspondingly higher density of states and the additional avoided crossings of the hyperspherical adiabats may increase the reactivity of these high-frequency modes.

The calculated vibrational term energies for reactant CD_3Br and product CD_3Cl, as obtained from the dimensionality-reduced model,[64] are listed in Table 2. The wavenumbers and quantum numbers of the reactants are primed to distinguish them from the product values. The anharmonic frequencies of the fundamental transitions of CD_3Br amount to $\nu_1' = 2197\ cm^{-1}$, $\nu_2' = 997\ cm^{-1}$, and $\nu_3' = 567\ cm^{-1}$. The corresponding experimental values[67] are 2151, 987, and 577 cm^{-1}, respectively. Compared to these values, the theoretical data show differences of −1.7, +1.0, and +2.1%, respectively. These small discrepancies are not only due to the potential but also due to the fact that the asymptotic energy of the PES is not yet reached at $\rho_{end} = 34\ a_0$ because of the long-range interaction of the fragments and because the treatment is somewhat approximate in this coordinate system where the hyperangle is used instead of the CH_3−Br distance.

The hyperspherical adiabatic curves are shown in Figure 1. The density of vibrational states is higher than in the $Cl^- + CD_3Br$ system, and the number of avoided crossing has increased. Note that only in the asymptotic region can a clear distinction between reactant and product adiabats be made.

Figure 2 gives an overview of the initial state-selected reaction probabilities summed over all product states, $P_i(E) = \sum_f P_{i,f}(E)$. The data are averaged over 80 cm^{-1} (at each point E, the interval $[E - \Delta, E + \Delta]$ with $\Delta = 40\ cm^{-1}$ is averaged) in this and in all following figures to smoothe the curves and thus to allow for a better comparison of the probabilities for varying initial vibrational excitation. Note that the original curves from our calculations, which are computed on a very fine energy grid, show extreme oscillations with very narrow resonance peaks. These fine resonances should not be confused with the broader resonance features still present in the figures after averaging.

Contrary to the nondeuterated reaction,[64] the probability vs energy functions do not form groups of curves of comparable orders-of-magnitude. All curves show an initial sharp rise with translational energy and then on average remain constant with some broader oscillations. However, neither a pronounced decrease nor an overall increase of $P(E)$ is observed, with the exceptions of the (0, 0, 1) curve and, to a lesser extent, the (0, 0, 3) curve. Over the translational energy interval up to 2800 cm^{-1}, the probability for reaction out of the vibrational ground state is fairly small, on average 2% and never exceeding 5%. This is surprising because the reaction is essentially net-barrierless. As expected from our experience,[59,64] excitation of the bond being broken, C−Br, strongly increases the reaction probability. There is an almost linear increase of the probability for initial excitation of ν_3, up to about 25% at $E_{trans} = 2300\ cm^{-1}$. Putting two quanta in this mode results in a strong enhancement of the reactivity, with a reaction probability that oscillates around 50%. With the reactant in the initial vibrational state (0, 0, 3) the probability rises up to 70%, and one more quantum increases this value to more than 75%. But even more quanta hardly can further increase the reactivity. The (0, 0, 5) curve is very close that for the initial state (0, 0, 4), and for higher excitation even a decrease is expected in accordance with our previous work on the reaction $Cl^- + CH_3Br$.[64] Due to the fact that the ν_1 and ν_2 values of the deuterated system are much lower than the corresponding quantities in CH_3Br, the density of states rises much steeper and the initial state with $\nu_3 = 6$ could not be included within justifiable computational effort (see section II).

Exciting the umbrella bend, ν_2, leads to a reaction probability of as much as 20% for small translational energies, whereas

TABLE 2: Assignment of Quantum Numbers ($v_1^{(}$, $v_2^{(}$, $v_3^{(}$) to the Initial and Final States of CD_3Br and CD_3Cl, Respectively

(v_1, v_2, v_3)	(v_1', v_2', v_3')	$E - E_{000}^{Cl}$	$E - E_{000}^{Br}$	(v_1, v_2, v_3)	(v_1', v_2', v_3')	$E - E_{000}^{Cl}$	$E - E_{000}^{Br}$
(0,0,0)		0.0			(0,0,3)	4315.9	1687.6
(0,0,1)		688.3		(2,0,0)		4375.2	
(0,1,0)		1040.3		(0,1,5)		4398.8	
(0,0,2)		1370.7		(0,3,2)		4421.5	
(0,1,1)		1724.3		(1,1,2)		4605.1	
(0,0,3)		2047.1			(0,2,0)	4611.3	1983.0
(0,2,0)		2061.6		(0,0,7)		4687.1	
(1,0,0)		2192.9		(0,4,1)		4745.6	
(0,1,2)		2402.4			(0,1,2)	4745.7	2117.4
	(0,0,0)	2628.3	0.0	(0,2,4)		4749.6	
(0,0,4)		2717.1			(1,0,0)	4825.7	2197.4
(0,2,1)		2742.5			(0,0,4)	4869.7	2241.4
(1,0,1)		2880.1		(1,0,4)		4905.6	
(0,3,0)		3071.8		(1,2,1)		4947.9	
(0,1,3)		3074.5		(0,1,6)		5051.2	
	(0,0,1)	3195.1	566.8	(2,0,1)		5059.5	
(1,1,0)		3248.3		(0,5,0)		5064.4	
(0,0,5)		3380.6		(0,3,3)		5087.0	
(0,2,2)		3417.3			(0,2,1)	5169.7	2541.4
(1,0,2)		3561.6		(1,1,3)		5274.1	
	(0,1,0)	3625.5	997.2	(1,3,0)		5282.8	
(0,1,4)		3739.7			(0,1,3)	5298.7	2670.4
(0,3,1)		3749.9		(0,0,8)		5329.8	
	(0,0,2)	3757.6	1129.3		(1,0,1)	5387.9	2759.6
(1,1,1)		3929.7		(0,2,5)		5403.0	
(0,0,6)		4037.3		(0,4,2)		5416.2	
(0,4,0)		4072.4			(0,0,5)	5419.1	2790.8
(0,2,3)		4085.9		(2,1,0)		5447.4	
	(0,1,1)	4188.0	1559.7	(1,0,5)		5567.6	
(1,0,3)		4236.8			(0,3,0)	5586.8	2958.5
(1,2,0)		4268.9					

[a] Here, $v_1^{(}$, $v_2^{(}$, and $v_3^{(}$ denote the C−D stretching, CD_3 umbrella bending and carbon−halogen stretching vibrations. Primed quantities refer to the reactants (CD_3Br). Energies $E - E_{000}^{Cl}$ (in cm^{-1}) are given with respect to the vibrational ground state of CD_3Cl, E_{000}^{Cl}, and for reactant states additionally with respect to the zero-point energy level of CD_3Br, E_{000}^{Br}.

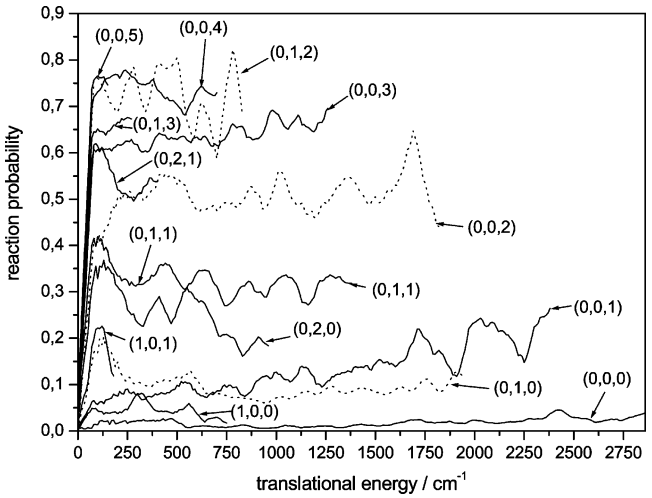

Figure 2. Initial state-selected reaction probabilities $P_i(E)$ for the exothermic reaction $Cl^- + CD_3Br$ (v_1', v_2', v_3') → $ClCD_3 + Br^-$ as functions of translational energy E_{trans}. The data are smoothed over intervals of 80 cm^{-1}. $P_{i,f}(E)$ is summed over all accessible product channels f to give $P_i(E)$.

this maximum rapidly decreases with E_{trans} and then remains at about 10%. At translational energies most relevant for the thermal rate constant, the influence of the umbrella bend is thus higher than that of the (0, 0, 1) mode. Two quanta in ν_2 yield a probability for reaction of about 35% at small E_{trans} that decreases for higher energies but still is more than twice as large as the probability for reaction out of state (0, 1, 0). The channel (0, 3, 0) opens just at the upper border of the total energy interval considered in this work (see Table 2).

Without any doubt, the symmetric C−D stretching mode is not a spectator, as can be seen from the factor >2 in the reaction probability compared to the ground state curve. The combination mode (1, 0, 1) shows a very high reactivity at small E_{trans}, once more highlighting the active role of the ν_1 mode in the dynamics.

As found in our previous studies on gas-phase S_N2 reactions,[59,60,64] the reactant combination mode of ν_2 and ν_3, which classically strongly resembles the harmonic transitional mode ω_4, yields a high reaction probability of about 30%, much more than the sum of the curves for initial states (0, 0, 1) and (0, 1, 0). Initial excitation of higher combination modes increases the reaction probability up to more than 80%. The hypothetical reactivity of 100% is not reached, due to the presence of the two potential wells that cause backscattering via the intermediately formed resonance states.

The probabilities for reaction of a chloride anion with either CH_3Br or CD_3Br are compared in Figure 3a,b. Obviously, the probability for reaction out of the vibrational ground state is higher for CD_3Br. This may be attributed to the higher density of states in the deuterated product system and to zero-point energy effects (see below) that influence the barrier height. A similar, but more pronounced, effect can be seen for initial excitation of the C−H or C−D stretching mode (see Figure 3a). A corresponding comparison for initial excitation of the C−Cl stretching, the umbrella and the (0, 1, 1) combination modes in both systems is given in Figure 3b. As the frequencies of the C−Br stretching modes are hardly affected by α-deuteration, the two (0, 0, 1) curves for CH_3Br and CD_3Br are very similar, with the latter probability being twice as large for small E_{trans}. Surprisingly, the reaction probability for exciting the CD_3 umbrella vibration is on average 5 times as large as that for

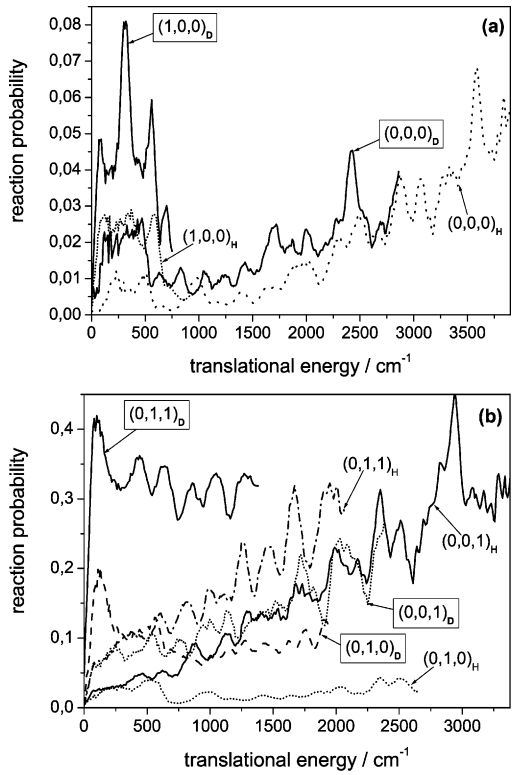

Figure 3. Initial state-selected reaction probabilities $P_i(E)$ for $Cl^- + CD_3Br$ (v'_1, v'_2, v'_3) → $ClCD_3 + Br^-$ compared with $Cl^- + CH_3Br$ (v'_1, v'_2, v'_3) → $ClCH_3 + Br^-$ as functions of translational energy E_{trans}. In (a), probabilities for reaction out of the ground state (0, 0, 0) and the state with one quantum in the C−H stretching mode (1, 0, 0) are compared, whereaes (b) contains excitation with one quantum in the C−Br stretch (0, 0, 1), the umbrella mode (0, 1, 0), and the combined mode (0, 1, 1). The data are smoothed over intervals of 80 cm^{-1}. $P_{i,f}(E)$ is summed over all accessible product channels *f*.

excitation of the corresponding CH_3 mode. This effect also influences the combination mode (0, 1, 1) which shows the already discussed high reaction probability at low translational energies.

The inverse kinetic isotope effect for the C−H stretching mode was not unexpected from our previous study on the $Cl^- + CD_3Cl'$ system[60] and an analysis of the vibrational frequency ω_1 in the course of reaction (see Table 1). On the basis of this argument, however, one would expect a "normal" KIE for the umbrella mode, as was found for the chlorine exchange reaction[60] because the vibrational frequency of the umbrella mode decreases when going from reactants to the transition state. In the system $Cl^- + CH_3Cl'$,[60] this contribution to a "normal" KIE was overcompensated by the effect arising from the C−D/C−H stretching vibration, resulting in an inverse KIE slightly below 1, as observed in the experiments.

To elucidate this effect more quantitatively and to demonstrate the nonstatistical character of the reaction under study, we performed a factor analysis of the vibrational contribution in the TST rate constant expression according to the work of Hu and Truhlar.[8] Here, η_{vib} is the vibrational contribution to the ratio k_H/k_D, defined as the product of individual contributions $\eta_{vib,i}$ of vibrational modes *i*, where

$$\eta_{vib,i}(T) = \frac{Q^{\dagger}_{i,H}(T)}{Q^{\dagger}_{i,D}(T)} \frac{Q_{i,D}(T)}{Q_{i,H}(T)} \qquad (3)$$

with $Q_{i,X}$ being the vibrational partition function of reactant (perprotio: X = H; perdeutero: X = D) or transition state (denoted by †),

$$Q_i(T) = \exp(-\hbar\omega_i/2k_BT)(1 - \exp(-\hbar\omega_i/k_BT))^{-1} \qquad (4)$$

with Boltzmann's constant k_B, at temperature *T*. Despite the triviality of this equation, we quote it here because the numerator is not self-evidently included but is crucial for the KIE because it determines the isotope-dependent shift of the reaction barrier height. The results for $T = 300$ K are reported in Table 3, where for the doubly degenerate modes also the squared factors $\eta^2_{vib,i}$ are given. Though TST is not applicable in its ordinary form due to the fact that the classical barrier height is below the corresponding reactant energy, we provide two sets of factors, one for the bimolecular reaction (superscript r in Table 3) and one for the unimolecular rearrangement starting from the intermediate complex $Cl^-\cdots CH_3Br$ (superscript c). Both data sets show the same trends. More accurate VTST calculations yield at lest qualitatively similar results for the KIE because the effect of a shifted transition state cancels out.[7,8] Inverse effects are found for the C−H stretches ω_1 and ω_5 as well as for the CH_3 rocking mode ω_7. The other modes, including the umbrella bend, contribute to a "normal" KIE. The product of all factors (squared for the degenerate modes) gives 0.955 in good are agreement with ref 2 where, however, a different set of vibrational frequencies (from semiempirical electronic structure calculations) was employed.

TABLE 3: Invidual Contributions of the Vibrational Modes to the Kinetic Isotope Effect at $T = 300$ K in the Reactions of $Cl^- + CH_3Br/CD_3Br$ [Superscript r(eactant)] and $Cl^-\cdots CH_3Br/CD_3Br$ [Superscript c(omplex)] to $ClCH_3/ClCD_3 + Br^-$ [a]

	$^r\eta_i$	$^r\eta_i^2$	$^c\eta_i$	$^c\eta_i^2$
ω_1	0.879		0.917	
ω_2	1.077		1.080	
ω_3	1.098		1.067	
ω_5	0.924	0.854	0.955	0.913
ω_6	1.108	1.228	1.069	1.142
ω_7	0.936	0.876	0.942	0.888
ω_8			1.013	1.025

[a] For details, see the text.

A quantitative comparison to the mode-selective KIE in our quantum study is not reasonable due to the quantitative inadequacy of the TST data and the questionable *J*-shifting-approximation that would be needed to convert our data to rate constants. Qualitatively, however, with regard to the above data, the strong enhancement of the reaction probability and the inverse KIE from the umbrella mode in $Cl^- + CD_3Br$ in our quantum scattering calculations demonstrates the nonstatistical behavior of the reaction under study, which is a general feature of S_N2 reactions with methyl halides.[5,7] An explanation for the inverse KIE of the umbrella mode is at a first glance difficult. Because the C−D umbrella mode stores less energy compared to its C−H counterpart, one would expect a smaller $P(E)$ as a function of translational energy. The reason is obviously the higher density of vibrational states in the product channel (see Table 2 and Figure 1); due to the exothermicity, this effect overcompensates the smaller energy stored in this mode: For the deuterated system, 18 product channels are available when the (0, 1, 0) mode opens up, whereas the corresponding number for the undeuterated system is 15. In the chlorine exchange reaction, however, deuteration causes the umbrella mode to have only one available product state instead of two for the first 300 cm^{-1} of translational energy.

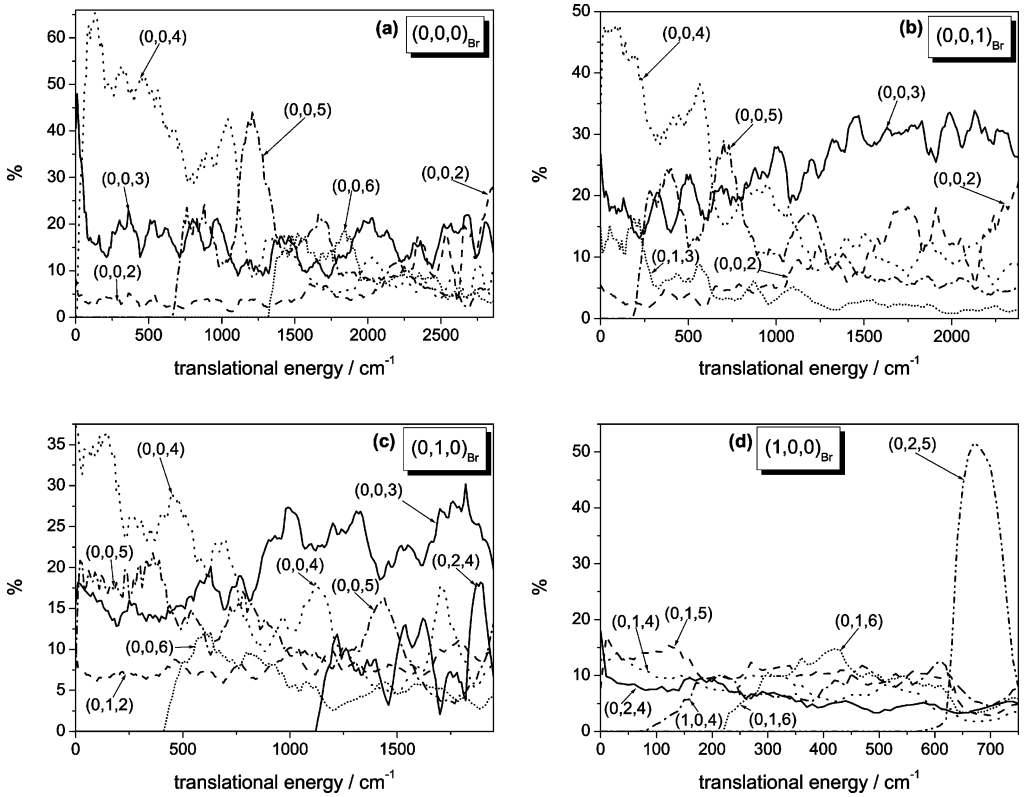

Figure 4. Product distributions for the exothermic reaction $Cl^- + CD_3Br$ (v_1', v_2', v_3') → $ClCD_3$ (v_1, v_2, v_3) + Br^- with (a) (v_1', v_2', v_3') = (0, 0, 0), (b) (v_1', v_2', v_3') = (0, 0, 1), (c) (v_1', v_2', v_3') = (0, 1, 0), and (d) (v_1', v_2', v_3') = (1, 0, 0). The data are smoothed over intervals of 80 cm^{-1}.

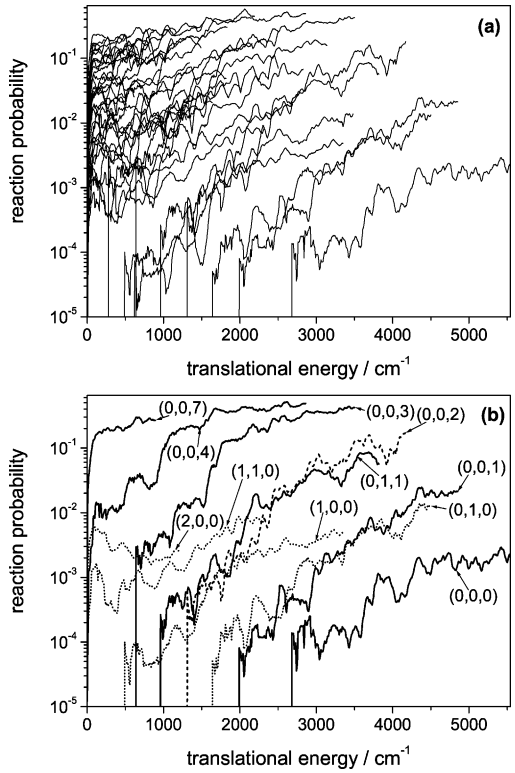

Figure 5. Initial state-selected reaction probabilities $P_i(E)$ for the endothermic reaction $Br^- + CD_3Cl$ (v_1, v_2, v_3) → $BrCD_3 + Cl^-$ as functions of translational energy E_{trans}. An overview of all computed state-selective reaction probabilities is given in (a), whereas (b) contains a selection of some relevant modes. The data are smoothed over intervals of 80 cm^{-1}. $P_{i,f}(E)$ is summed over all accessible product channels *f*.

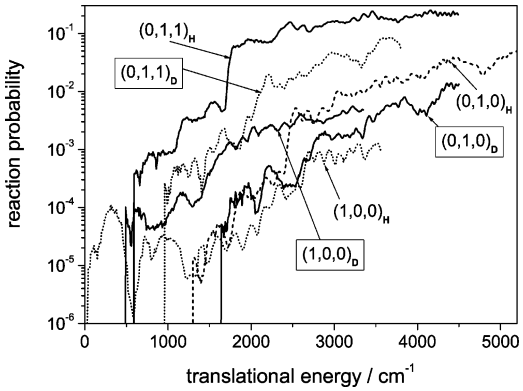

Figure 6. Initial state-selected reaction probabilities $P_i(E)$ for $Br^- + CD_3Cl$ (v_1, v_2, v_3) → $BrCD_3 + Cl^-$ compared with $Br^- + CH_3Cl$ (v_1, v_2, v_3) → $BrCH_3 + Cl^-$ as functions of translational energy E_{trans}. The data are smoothed over intervals of 80 cm^{-1}. $P_{i,f}(E)$ is summed over all accessible product channels *f*.

But the reason for the inverse KIE is also found in the importance of tunneling in the gas-phase S_N2 reaction that was already stressed in a previous two-dimensional quantum study on $Cl^- + CH_3Br$ by Schmatz et al.[54] In the heavy−light−heavy halogen-exchange reaction, the two halogen atoms may be assumed to be fixed. Then, the S_N2 process reduces to the inversion of the methyl group, similar to the well-known NH_3 inversion. Clearly, the hydrogen atoms play the key role in this process, which is subject to tunneling and strongly mass-dependent. In the net-barrier-less reaction $Cl^- + CH_3Br$, tunneling plays only a very minor role in reactive processes, rendering the mass-dependent effect negligible. In the barrier-dominated chlorine exchange, however, H/D substitution strongly affects the tunneling in the inversion process of CH_3/CD_3 and decreases the reactivity. Furthermore, the energetic reason for the "normal" KIE, viz. raising the reaction barrier through vibrational effects, is not so important in the Cl/Br exchange due to the lack of a net barrier. Note that tunneling is intrinsically

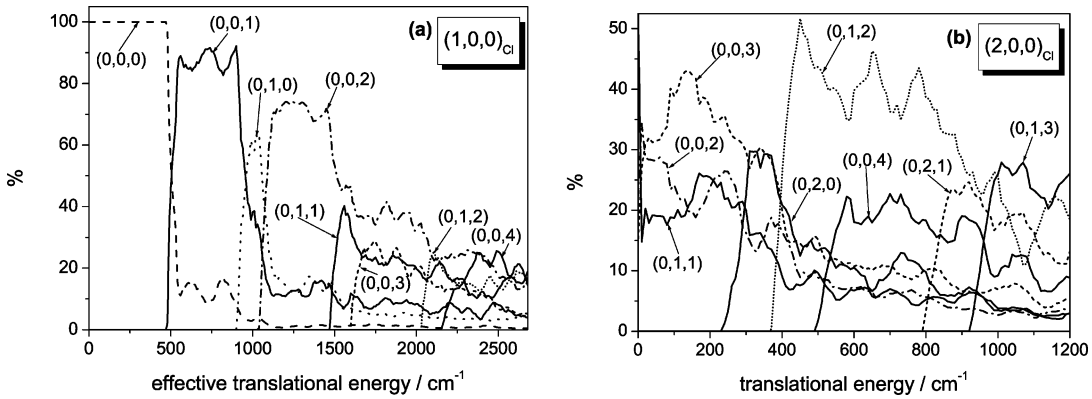

Figure 7. Product distributions for the endothermic reaction $Br^- + CD_3Cl$ (v_1, v_2, v_3) → $BrCD_3$ (v_1', v_2', v_3') + Cl^- with (a) (v_1, v_2, v_3) = (1, 0, 0) and (b) (v_1, v_2, v_3) = (2, 0, 0). The data are smoothed over intervals of 80 cm^{-1}.

included in our quantum scattering calculations, whereas TST needs additional factors to account for this effect.

Finally, product distributions for the reaction between Cl^- and CD_3Br in selected initial vibrational states are graphically displayed in Figure 4a−d. The distributions are obtained as normalized state-to-state reaction probabilities, $P_{i,f}(E)/P_i(E)$. Product states with negligible populations are not shown in the figures.

Initial state (0, 0, 0) (cf. Figure 4a) prefers product states with the ν_3-mode excited, whereby states (0, 0, 2) and (0, 0, 3) dominate. Overall, we find a gain of translational energy due to the exothermicity. However, relative to the reactants, the products are vibrationally hot. For reaction out of CH_3Br state (0, 0, 1) (Figure 4b), the product states (0, 0, 2) and (0, 0, 3) are most important. Because in both cases the α-H substitution-dependent modes are not involved, this picture, which is very similar to that in the $Cl^- + CH_3Br$ reaction, is expected.

Reaction with one quantum in the umbrella bend (Figure 4c) results in strong vibrational excitation of the C−Cl stretch ν_3 in the product molecule. The energy originally stored in this mode is almost completely released into other vibrations; only the (0, 1, 2) level is populated almost constantly with about 10%, whereas for translational energies larger than 1100 cm^{-1} also the combination mode (0, 2, 4) becomes important. Compared to the $Cl^- + CH_3Br$ system, large contributions from combination product states, like (0, 1, 2) and (0, 1, 3) are missing. The preference of pure ν_3 excitation in the products again highlights that the umbrella bending mode is a very active mode in the reaction.

Finally, reaction out of initial state (1, 0, 0) (Figure 4d) exhibits a strong release of vibrational energy into the other two modes. Only a small percentage of about 10% remains in the C−D stretch. Centered at about 670 cm^{-1} of translational energy, a remarkable peak in the state-selected probability into product state (0, 2, 5) shows up, which is an artifact from the scattering calculations. It can be traced back to an avoided crossing of the curves $(1, 0, 1)_{Br}$ and $(0, 2, 5)_{Cl}$ very far out in the asymptotic region (at $\rho \approx 31.6\ a_0$). This artifact occurs after opening of the "reactively excited counterpart" of initial state $(1, 0, 0)_{Br}$, the $(1, 0, 1)_{Br}$ mode, at 567 cm^{-1} translational energy. Remarkably, no products with pure ν_3 excitation are formed, contrary to the $Cl^- + CH_3Br$ system.

In ref 64, we have compared the probabilities for the reactions of a chloride anion with CH_3Cl and CH_3Br. It is now interesting to compare the reaction of Cl^- with either CD_3Cl or CD_3Br. For brevity, no figure is provided and only a verbal description is given. Qualitatively, the curves for initial (0, 0, 0) and (1, 0, 0) states show the same behavior for both CD_3Br and CD_3Cl. The only difference is that the onset of spectator-like behavior is shifted to larger translational energies in the deuterated systems, due to the fact that ν_1 is smaller and that this mode can thus significantly contribute to the reaction probability also for larger E_{trans}. For the initial state (0, 1, 0), however, we find that the reactivity with CD_3Br is by more than an order of magnitude higher than with CD_3Cl whereas in the nondeuterated systems both curves were very similar to each other. The reason for this effect was discussed above.

B. Endothermic Reaction $Br^- + CD_3Cl$. In Figure 5, the initial state selected reaction probabilities are shown for the reverse, endothermic reaction $Br^- + CD_3Cl \rightarrow BrCD_3 + Cl^-$. While Figure 5a provides an overview of the distribution and the convergence behavior of the state-selected probabilities, Figure 5b gives a detailed assignment of the most important initial states. The scales are logarithmic, and the channels for all initial CH_3Cl states that are energetically below the (0, 0, 0) level of CH_3Br open only if the available translational energy matches that value. As a consequence, the reaction probability out of the ground state is very low. Excitation of either umbrella bend or the C−Cl stretch with one quantum each results in very similar reaction probabilities, indicating that the energy stored in these modes is only used to overcome the endothermicity by energy redistribution in the collision complexes. There is thus no mode-selectivity observed. The same holds for the C−H stretch which, due to its higher frequency, is more capable of enhancing the reactivity. The combination mode (0, 1, 1), however, is very effective in promoting the reaction due to the close similarity with the transitional mode.

The higher initial states, which are asymptotically above the CH_3Br (0, 0, 0) level, show reaction probabilities on the order of 10 to 50%. In particular, initially highly excited states in ν_3 lead to high reaction probabilities. Also the combination mode (1, 1, 0) and the first overtone of the ν_1 mode, (2, 0, 0), have large reaction probabilities, contrary to the once well-established spectator-mode concept. Note that in the $Br^- + CD_3Cl$ reaction, the (2, 0, 0) curve covers a larger translational energy interval than the corresponding curve in the $Cl^- + CH_3Br$ reaction due to the lower ν_1 frequency.

In Figure 6, the probabilities of the three modes that are most influenced by α-H-substitution are compared for the reactions of a bromine anion with either CH_3Cl or CD_3Cl. The deuteration increases the reactivity out of state (1, 0, 0), but decreases it if the umbrella mode or the corresponding combination with ν_3 is excited. This is the typical inverse effect for the C−H stretches and the "normal" effect for the umbrella bend for barrier-dominated or endothermic reactions, as already reported for $Cl^- + CH_3Cl'$ in ref 60. It is remarkable that the "normal" KIE for

$Br^- + CH_3Cl/CD_3Cl$ and the "anomalous" behavior in the exothermic reverse reaction $Cl^- + CH_3Br/CD_3Br$ are found in the *same* system.

A closer look at the product distributions may reveal interesting details on the high-frequency ν_1-modes. Figure 7a gives the product distribution for initial CD_3Cl state (1, 0, 0); despite their different character, the other initial states below the CD_3Br ground state show a very similar behavior and are not included for brevity. As is common for endothermic or barrier-dominated S_N2 reactions, the energetically highest products are most likely formed.[59,60,64] Whenever a new channel opens up, the corresponding asymptotic state becomes dominating. The same finding was made in the chlorine-exchange reaction[59] and in the undeuterated system.[64] As a consequence of this behavior, the energy stored in the C−H stretch completely leaves this mode. Despite the fact that the adiabaticity of this mode, i.e., conservation of the ν_1' excitation, is impossible for energetic reasons up to 2630 cm^{-1} of translational energy, the mode is very active, populating the umbrella and, most importantly, the newly formed C−Br stretch. If there were adiabatic, "spectator"-like behavior of the ν_1 mode, one should expect that the reactant (2, 0, 0) (see Figure 7b) ends up in an (1, *m*, *n*) product level above 450 cm^{-1} of translational energy. However, this is not observed. The complete energy originally stored in ν_1 is released into ν_2 and ν_3 product vibrations.

IV. Conclusions

Employing a CCSD(T) potential energy surface, time-independent quantum-scattering calculations up to 2960 cm^{-1} above the vibrational ground state of the reactant molecule have been carried out on the exothermic gas-phase S_N2 reaction $Cl^- + CD_3Br \rightarrow ClCD_3 + Br^-$ and the endothermic counterpart $Br^- + CD_3Cl \rightarrow BrCD_3 + Cl^-$. Hyperspherical coordinates were used to describe the bonds being broken and formed, and the two totally symmetric modes of the methyl group, symmetric C−D stretching and umbrella bending, are explicitly included in the model. A very narrow grid in the total energy was employed so that long living resonance states could be resolved. Initial state selected reaction probabilities and product distributions as a function of translational energy are analyzed and discussed in detail.

The experimentally observed inverse secondary kinetic isotope effect is confirmed in our quantum-mechanical scattering calculations. Compared to the undeuterated system, the initial state-selected reaction probability shows an enhancement of the reactivity when the symmetric C−D stretching mode is excited. This is in line with the estimates from transition state theory that predicts a higher rate constant due to a lower effective barrier. Although TST yields a "normal" KIE for the umbrella mode excited, our calculations give strong evidence for a considerable increase of the reaction probability, i.e., an inverse effect, in the deuterated system. This anomalous, nonstatistical behavior is contrary to chemical intuition, because (a) the effective barrier becomes higher upon deuteration, (b) the tunneling probability should be much lower in the deuterated system, and (c) the available internal energy is lower due to the smaller vibrational frequency. However, the increased density of states and the correspondingly higher number of avoided crossings of the hyperspherical adiabats obviously strongly increase the reactivity. Tunneling does not play any significant role in the $Cl^- + CH_3Br/CD_3Br$ system because the barrier is below the classical reactant energy. In the $Cl^- + CH_3Cl'/CD_3Cl'$ system,[60] however, tunneling is important and consequently decreases the reaction probability out of state (0, 1, 0) when H is substituted by D. In the reverse endothermic reaction $Br^- + CD_3Cl$, the kinetic isotope effect of the umbrella mode is normal. Both reaction probabilities, for reaction 1 and its reverse, are obtained from the same **S** matrix, indicating that the reported effect has a physical reason and is not an artifact. The inverse, nonstatistical KIE for the umbrella mode in the exothermic reaction might be one reason for several reported TST values for the KIE to be too close to unity. TST also predicts the antisymmetric counterpart of the umbrella mode, the doubly degenerate antisymmetric C−H bending mode (ω_6) to have a normal KIE. If we assume a qualitatively similar behavior of the symmetric and the corresponding antisymmetric modes,[65] this may yield another contribution to the inverse KIE that is not correctly represented by TST.

Acknowledgment. This work was financially supported by the Deutsche Forschungsgemeinschaft (DFG) through grant SCHM 1651/1. Additional support from the Fonds der chemischen Industrie is gratefully acknowledged.

Note Added after ASAP Publication. This article was released ASAP on November 8, 2005. In Table 1, column 2 has been revised. The correct version was posted on November 11, 2005.

References and Notes

(1) Gronert, S.; DePuy, C. H.; Bierbaum, V. M. *J. Am. Chem. Soc.* **1991**, *113*, 4009.
(2) Viggiano, A. A.; Paschkewitz, J. S.; Morris, R. A.; Paulson, J. F.; Gonzales-Lafont, A.; Truhlar, D. G. *J. Am. Chem. Soc.* **1991**, *113*, 9404.
(3) Viggiano, A. A.; Morris, R. A.; Paschkewitz, J. S.; Paulson, J. F. *J. Am. Chem. Soc.* **1992**, *114*, 10477.
(4) O'Hair, R. A. J.; Davico, G. E.; Hacaloglu, J.; Dang, T. T.; DePuy, C. H.; Bierbaum, V. M. *J. Am. Chem. Soc.* **1994**, *116*, 3609.
(5) Kato, S.; Davico, G. E.; Lee, H. S.; DePuy, C. H.; Bierbaum, V. M. *Int. J. Mass Spectrosc.* **2001**, *210/211*, 223.
(6) Craig, S. L.; Brauman, J. I. *J. Phys. Chem. A* **1997**, *101*, 4745.
(7) Wang, H.; Hase, W. L. *J. Am. Chem. Soc.* **1995**, *117*, 9347.
(8) Hu, W. P.; Truhlar, D. G. *J. Am. Chem. Soc.* **1995**, *117*, 10726.
(9) Zhao, X. G.; Tucker, S. C.; Truhlar, D. G. *J. Am. Chem. Soc.* **1991**, *113*, 826.
(10) Gonzales-Lafont, A.; Truong, T. N.; Truhlar, D. G. *J. Phys. Chem.* **1991**, *95*, 4618.
(11) Zhao, X. G.; Lu, D.-H.; Liu, Y.-P.; Lynch, G. C.; Truhlar, D. G. *J. Chem. Phys.* **1992**, *97*, 6369.
(12) Streitwieser, A., Jr.; Jagow, R. H.; Fahey, R. C.; Suzuki, S. *J. Am. Chem. Soc.* **1958**, *80*, 2326.
(13) Llewellyn, J. A.; Robertson, R. E.; Scott, J. W. M. *Can. J. Chem.* **1960**, *38*, 222.
(14) Weston, R. E., Jr. *Annu. Rev. Nucl. Sci.* **1961**, *11*, 439.
(15) Seltzer, S.; Zavitsas, A. A. *Can. J. Chem.* **1967**, *45*, 2023.
(16) Willi, A. V.; Wom, C. M. *J. Am. Chem. Soc.* **1968**, *90*, 5999.
(17) Scheppele, S. E. *Chem. Rev.* **1972**, *72*, 511.
(18) Melander, L.; Saunders, W. H. *Reaction Rates of Isotopic Molecules*; Wiley: New York, 1980.
(19) Yamataka, H.; Tamura, S.; Hanafusa, T.; Ando, T. *J. Am. Chem. Soc.* **1985**, *107*, 5429.
(20) Saunders, W. H., Jr. In *Investigation of Rates and Mechanism of Reactions*; Bernasconi, C. F., Ed.; Wiley: New York, 1986; Part I, p 565.
(21) Olmstaed, W. N.; Brauman, J. I. *J. Am. Chem. Soc.* **1977**, *99*, 4219.
(22) Dodd, J. A.; Brauman, J. I. *J. Phys. Chem.* **1986**, *90*, 3559.
(23) Barlow, S. E.; VanDoren, J. M.; Bierbaum, V. M. *J. Am. Chem. Soc.* **1988**, *110*, 7240.
(24) Brauman, J. I. *J. Mass Spectrom.* **1995**, *30*, 1649.
(25) DeTuri, V. F.; Hintz, P. A.; Ervin, K. M. *J. Phys. Chem.* **1997**, *101*, 5969.
(26) Chabinyc, M. L.; Craig, S. L.; Regan, C. K.; Brauman, J. I. *Science* **1998**, *279*, 1882.
(27) Ervin, K. M. *Int. J. Mass Spectrom.* **1999**, *187*, 343.
(28) Angel, L. A.; Ervin, K. M. *J. Phys. Chem. A* **2001**, *105*, 4042.
(29) Kato, S.; Davico, G. E.; Lee, H. S.; Depuy, C. H.; Bierbaum, V. M. *Int. J. Mass Spectrom.* **2001**, *210/211*, 223.
(30) Angel, L. A.; Garcia, S. P.; Ervin, K. M. *J. Am. Chem. Soc.* **2002**, *124*, 336.
(31) Angel, L. A.; Ervin, K. M. *J. Am. Chem. Soc.* **2003**, *125*, 1014.

(32) Wester, R.; Bragg, A. E.; Davis, A. V.; Neumark, D. M. *J. Chem. Phys.* **2003**, *119*, 10032.
(33) Angel, L. A.; Ervin, K. M. *J. Phys. Chem. A* **2004**, *108*, 9827.
(34) Vande Linde, S. R.; Hase, W. L. *J. Phys. Chem.* **1990**, *94*, 2778.
(35) Vande Linde, S. R.; Hase, W. L. *J. Chem. Phys.* **1990**, *93*, 7962.
(36) Cho, Y. J.; Vande Linde, S. R.; Zhu, L.; Hase, W. R. *J. Chem. Phys.* **1992**, *96*, 8275.
(37) Hase, W. L.; Cho, Y. J. *J. Chem. Phys.* **1993**, *98*, 8626.
(38) Hase, W. L. *Science* **1994**, *266*, 998.
(39) Peslherbe, G. H.; Wang, H.; Hase, W. L. *J. Chem. Phys.* **1995**, *102*, 5626.
(40) Peslherbe, G. H.; Wang, H.; Hase, W. L. *J. Am. Chem. Soc.* **1996**, *118*, 257.
(41) Wang, H.; Goldfield, E. M.; Hase, W. L. *J. Chem. Soc., Faraday Trans.* **1997**, *93*, 737.
(42) Clary, D. C.; Palma, J. *J. Chem. Phys.* **1997**, *106*, 575.
(43) Schmatz, S.; Clary, D. C. *J. Chem. Phys.* **1998**, *109*, 8200.
(44) Mann, D. J.; Hase, W. L. *J. Phys. Chem. A* **1998**, *102*, 6208.
(45) Su, T.; Hase, W. L. *J. Phys. Chem. A* **1998**, *102*, 9819.
(46) Li, G. S.; Hase, W. L. *J. Am. Chem. Soc.* **1999**, *121*, 7124.
(47) Schmatz, S.; Clary, D. C. *J. Chem. Phys.* **1999**, *110*, 9483.
(48) Hernández, M. I.; Campos-Martinez, J.; Villarreal, P.; Schmatz, S.; Clary, D. C. *Phys. Chem. Chem. Phys.* **1999**, *1*, 1197.
(49) Yu, H. G.; Nyman, G. *Chem. Phys. Lett.* **1999**, *312*, 585.
(50) Schmatz, S. *Chem. Phys. Lett.* **2000**, *330*, 188.
(51) Schmatz, S.; Botschwina, P.; Hauschildt, J.; Schinke, R. *J. Chem. Phys.* **2001**, *114*, 5233.
(52) Song, K. Y.; Sun, L. P.; Hase, W. L. *J. Am. Chem. Soc.* **2001**, *123*, 5753.
(53) Hauschildt, J.; Schinke, R.; Schmatz, S.; Botschwina, P. *Phys. Chem. Chem. Phys.* **2001**, *3*, 2275.
(54) Schmatz, S.; Botschwina, P.; Hauschildt, J.; Schinke, R. *J. Chem. Phys.* **2002**, *117*, 9710.
(55) Laerdahl, J. K.; Uggerud, E. *Int. J. Mass Spectrom. Ion Processes* **2002**, *214*, 277.
(56) Schmatz, S.; Hauschildt, J. *J. Chem. Phys.* **2003**, *118*, 4499.
(57) Wang, Y.; Hase, W. L.; Wang, H. *J. Chem. Phys.* **2003**, *118*, 2688.
(58) Schmatz, S. *Chem. Phys. Chem.* **2004**, *5*, 600.
(59) Hennig, C.; Schmatz, S. *J. Chem. Phys.* **2004**, *121*, 220.
(60) Botschwina, P.; Hennig, C.; Schmatz, S. *Phys. Chem. Chem. Phys.* **2004**, *6*, 4630.
(61) Sun, L. P.; Chang, E. Y.; Song, K. Y.; Hase, W. L. *Can. J. Chem.* **2004**, *82*, 891.
(62) Hennig, C.; Schmatz, S. *Phys. Chem. Chem. Phys.* **2005**, *7*, 1100.
(63) Schmatz, S. *J. Chem. Phys.* **2005**, *122*, no. 234306.
(64) Hennig, C.; Schmatz, S. *J. Chem. Phys.* **2005**, *122*, no. 234307.
(65) Hennig, C.; Schmatz, S. *J. Phys. Chem. A*, in press.
(66) Hase, W. L. In *Encyclopedia of Mass Spectrometry*; Caprioli, R., Gross, M., Eds.; Elsevier: Amsterdam, 2005; Vol. 4, pp 504.
(67) Herzberg, G. *Molecular Spectra and Molecular Structure. IInfrared, I.; Raman Spectra of Polyatomic Molecules;* Van Nostrand Reinhold: New York, 1945.
(68) Schmatz, S.; Stoll, H.; Botschwina, P. *Int. J. Mass Spectrosc.* **2000**, *201*, 277.